



Vol. 26, No 1, 2
Enero - Junio 2018

CIENTIFICA



An International Refereed Scientific Journal
of the Facultad Experimental de Ciencias
at the Universidad del Zulia

Esta publicación científica en
formato digital es continuidad
de la revista impresa

Depósito Legal: pp 199302ZU47

ISSN: 1315-2076

CIENCIA 26 (1,2), 28 - 41, 2018
Maracaibo, Venezuela

Effect of Sn addition in alumina- and silica-supported palladium catalysts for n-butane dehydrogenation (Dehydrogenation of n-butane over supported palladium catalysts)

*Jonathan E. Mendez **, *Douglas R. Rodríguez*, *Jorge L. Sánchez*, *Geomar J. Arteaga*.

Instituto de Superficies y Catálisis, Facultad de Ingeniería, Universidad del Zulia, P. O. Box 15251,
Maracaibo 4003A, Venezuela.

Recibido: 15-01-18 Aceptado: 06-02-18

Abstract

Dehydrogenation of n-butane was studied over alumina- and silica-supported Pd and Pd-Sn catalysts with 0.5 wt. % of Pd. The reaction was carried out at 500 °C in both continuous flow and pulses systems. The catalysts were prepared by incipient wetness impregnation. For the bimetallic catalysts, the sequential impregnation method was used adding first Sn and then Pd, with Sn/Pd atomic ratios of 0.1, 0.25 and 0.5. The samples were characterized by XRF, UV-DRS, N₂ adsorption, TPR, CO chemisorption and FTIR-CO techniques. On the supported-alumina catalysts, Pd oxychloride were formed, which is highly resistant to the reduction, and it is responsible for the high Pd dispersion. On the supported-silica catalysts, the addition of Sn modifies both the reducibility and adsorption capacity of Pd. The effects of Sn were mainly of geometric nature when supported on alumina, and both geometric and electronic nature when supported on silica. On the supported-alumina catalysts, the Sn addition increases the selectivity toward butenes, due to the high stabilization of Pd species; while on the supported-silica catalysts, greater Pd-Sn interactions are evidenced, where the catalyst properties are strongly influenced at the lowest content of Sn added. The alumina-supported bimetallic catalysts showed the best performance for n-butane dehydrogenation among the catalysts investigated herein.

Keywords: Palladium-tin catalysts; Sn/Pd ratio; FTIR-CO; n-butane dehydrogenation.

Efecto de la adición de estaño en catalizadores de paladio soportados sobre alúmina y sílice para la deshidrogenación de n-butano (Deshidrogenación de n-butano en catalizadores de paladio soportado)

Resumen

Se estudió la deshidrogenación del n-butano en catalizadores de Pd y Pd-Sn soportados sobre alúmina y sílice, con una carga de Pd de 0,5 % p/p. La reacción se llevó a cabo a 500 ° C tanto en flujo continuo como por pulsos. Los catalizadores fueron preparados mediante impregnación a humedad incipiente. Para los catalizadores bimetalicos, se utilizó la impregnación secuencial, añadiendo primero Sn y luego Pd, para obtener relaciones atómicas Sn/Pd nominales de 0,1, 0,25 y 0,5. Las muestras se caracterizaron mediante las técnicas de XRF, UV-DRS, adsorción de N₂, TPR, quimisorción de CO y FTIR-CO. En los catalizadores soportados sobre alúmina, se formó un complejo de oxicloriguro de Pd, que es altamente resistente a la reducción y es responsable de la alta dispersión de Pd. En los catalizadores soportados sobre sílice, la adición de Sn modificó tanto la reducibilidad como la capacidad de adsorción del Pd. Los efectos del Sn sobre el Pd fueron principalmente del tipo geométrico en los catalizadores soportados sobre alúmina, y de naturaleza tanto geométrica como electrónica en aquellos soportados sobre sílice. En los catalizadores soportados sobre alúmina, la adición de Sn aumentó la selectividad, debido a la alta estabilidad de las especies de Pd; mientras que en los catalizadores soportados sobre sílice, se evidenciaron mayores interacciones Pd-Sn, donde las propiedades de los catalizadores se vieron fuertemente influenciadas con el menor contenido de Sn adicionado. Los catalizadores bimetalicos soportados sobre alúmina mostraron el mejor desempeño para la deshidrogenación de n-butano.

* Corresponding Author: Tel-fax.: +58 (261) 4128791/97. E-mail: jomendez@fing.luz.edu.ve.
Other E-mail addresses: dorodriguez@fing.luz.edu.ve, jlsanchez@fing.luz.edu.ve, garteaga@fing.luz.edu.ve

Palabras Claves: Catalizadores de paladio-estaño; relación Sn/Pd; FTIR-CO; Deshidrogenación de n-butano.

Introduction

The importance of catalytic dehydrogenation of light paraffins to olefins has been growing due to the demand for these unsaturated hydrocarbons [1]. They are the starting material for some of the most important chemical products, such as polymers, synthetic rubbers and oxygenated compounds for reformulated fuels. Unfortunately, light olefins are not available as a natural resource; they are obtained in stream cracking furnaces and produced in FCC (fluid catalytic cracking) plants in refineries. Catalytic dehydrogenation of light paraffins (like the widely available normal-butane) provides a second way to obtain light olefins, which in turn can be transformed into more valuable chemicals, including the methyl tertiary-butyl ether (MTBE), ethyl tertiary-butyl ether (ETBE), and tertiary amyl methyl ether (TAME) [1-3].

Nevertheless, the conversion of light paraffins to the corresponding olefins is limited by thermodynamics restrictions due to the strong endothermic character of this reaction. High temperatures (530–730 °C) are required to reach conversions of nearly 50% for paraffins C₂–C₆. The dehydrogenation temperatures are higher for light paraffins than for heavy ones [1].

Side reactions like isomerization, thermal cracking and coking, which are thermodynamically and kinetically favoured over dehydrogenation reactions, can occur under operating conditions (>530 °C). Therefore, it is highly desirable a catalyst with a suitable conversion and high selectivity towards the desired olefin, working at lower reaction temperatures. Besides, the unavoidable formation of coke on the catalyst surface that results in a progressive reduction of catalytic activity, could be minimized at these more benevolent conditions [2]. The use of weak acid supports in a catalytic system is also essential to avoid side reactions, like cracking and isomerization.

Many researchers have been devoted to study the dehydrogenation of light paraffins over Pt-based catalysts, particularly on bimetallic Pt-Sn supported catalyst [4-8], due to the beneficial effects of tin as a promoter: tin decreases the size of platinum ensembles; reducing hydrogenolysis and coking that require large ensembles of platinum, and/or acts as electronic modifier of Pt, thereby enhancing the catalyst selectivity and stability. However, few studies are related to the performance of these reactions on supported Pd catalysts [1, 9-11]. Particularly, the Pd-Sn system has been studied for nitrates removal [12, 13], methane oxidation [14, 15] and selective hydrogenation reactions [16-18].

A catalytic system based on Pd can be an alternative to the more expensive metals for dehydrogenation reactions, such as Pt, Ru and Ir. Studies carried out earlier [9] on the performance of Pd-Sn/SiO₂ catalysts for propane dehydrogenation, revealed the effects of tin addition in low proportions (Sn/Pd atomic ratio = 0.14-0.84), and an optimal in both adsorption capacity of Pd and catalytic activity was found. Rodriguez et al. [1] studied the n-butane dehydrogenation over Pd-Ga/Al₂O₃ catalysts with different atomic Ga/Pd ratios, and they found that the effects of Ga were the same as those caused by Sn for dehydrogenation in Pd-Sn/Al₂O₃ catalysts.

The aim of this work is to study the effect of Sn/Pd ratio on the catalytic properties of supported Pd catalysts for n-butane dehydrogenation reaction in both continuous flow and pulses at a relatively low temperature (500 °C). Alumina and silica were chosen as support due to its low acid strength, in order to do not promote cracking reactions that affect selectivity towards olefins. Catalysts were characterized by X-ray fluorescence spectroscopy (XRF), diffuse reflectance UV-vis spectroscopy (UV-DRS), N₂ adsorption, temperature programmed reduction (TPR), CO chemisorption and FTIR spectroscopy of adsorbed CO (FTIR-CO).

Experimental

Catalysts preparation

Monometallic Pd and Sn samples were prepared by incipient wetness impregnation of γ -Al₂O₃ (Alfa Aesar, SBET = 210 m²/g, V_{pore} = 0.76 cm³/g) and SiO₂ (Cabosil M-5, Scintran, SBET = 224 m²/g), using a rotavapor at 80 °C, with an aqueous solution of PdCl₂ (Fisher Scientific, 99%) or SnCl₄·5H₂O (Fisher Scientific, > 99%) in HCl, in order to obtain Pd and Sn nominal contents of 0.5 and 0.56 wt. %, respectively. Bimetallic Pd-Sn/Al₂O₃ and Pd-Sn/SiO₂ catalysts were prepared by sequential impregnation, adding first Sn and then Pd. Supports were previously crushed and sieved (60/80 mesh), and then calcined at 700 °C for 4 h. The nominal contents of metals in bimetallic catalysts were 0.5 wt. % Pd and 0.056–0.28 wt. % Sn, (Sn/Pd atomic ratios between 0.1 and 0.5). After impregnating, the samples were dried at 120 °C overnight, and then calcined at 500 °C for 2 h. Pd, Sn and Cl contents were measured by energy dispersive X-ray fluorescence spectroscopy (XRF) using a Shimadzu EDX-700HS spectrometer, provided with an Rh gun operated at 50 keV. Al₂O₃ and SiO₂ supports will be named Al and Si, respectively. Table 1 summarizes the notation and chemical composition of the catalysts.

Table 1. Chemical composition, surface area and CO/Pd ratio

Catalysts	Pd (wt. %)	Sn (wt. %)	Cl (wt.%)	Sn/Pd atomic ratio	S _{BET} (m ² /g)	CO/Pd ^a
Pd _{0.40} Al	0.40	-	0.70	0	-	0.56
Pd _{0.55} Sn _{0.045} Al	0.55	0.045	0.54	0.073	210	0.53
Pd _{0.52} Sn _{0.091} Al	0.52	0.091	0.58	0.16	-	0.58
Pd _{0.54} Sn _{0.19} Al	0.54	0.19	0.66	0.32	215	0.51
Sn _{0.43} Al	-	0.43	0.70	∞	-	-
Pd _{0.34} Si	0.34	-	n.d.	0	-	0.20
Pd _{0.31} Sn _{0.061} Si	0.31	0.061	n.d.	0.18	218	0.08
Pd _{0.36} Sn _{0.12} Si	0.36	0.12	n.d.	0.30	-	0.09
Pd _{0.31} Sn _{0.22} Si	0.31	0.22	n.d.	0.64	218	0.06
Sn _{0.51} Si	-	0.51	n.d.	∞	-	-

n.d.: not detected

a: Based on the Pd loading values obtained by XRF.

Characterization techniques

BET surface areas of supports and catalysts were determined from the N₂ adsorption isotherms at -196 °C, using an automatic Micromeritics ASAP 2010 apparatus after the samples were outgassed at 150 °C for 2 h. The specific surface area of selected catalysts are also listed in Table 1.

The catalysts were studied by UV-vis diffuse reflectance spectroscopy (UV-DRS) at atmospheric conditions, in a Perkin-Elmer spectrometer model Lambda 2 equipped with a diffuse reflectance accessory, consisting of an integrating sphere of 50 mm coated with BaSO₄ to collect the reflected light. The wavelength range varied from 190 to 700 nm.

TPR profiles were measured from -50 to 700 °C in a Vycor U-tube reactor connected to a stainless steel apparatus provided with a thermal conductivity detector (TCD), using a mixture of 5% H₂/Ar as reducing gas. Prior to measurements, the sample (100 mg) was pretreated in air flow at 500 °C for 1 h, then cooled down in flowing Ar to room temperature and, then, to -50 °C, using an isopropanol-liquid nitrogen bath, before admitting the flow of reducing gas. The reactor was freely heated from -50 to room temperature (RT) by removing the cool bath, and immediately heated up to 700 °C at 10 °C/min, using a temperature-controlled furnace.

Dynamic CO chemisorption measurements were carried out in the same stainless steel apparatus used in TPR experiments, which was equipped with a gas injection valve (Valco). Successive CO pulses (58 μL STP) were sent to the reactor until reaching

the saturation, using He (30 mL/min) as carrier gas. The catalysts (100 mg) were previously reduced at 400 °C in flowing H₂ for 1 h, and then the adsorbed hydrogen was removed by flushing He at the same temperature for 1 h.

Fourier transform infrared spectra of adsorbed CO (FTIR-CO) were recorded at RT on a Shimadzu IR Prestige 21 spectrometer, at a resolution of 2 cm⁻¹ using around 100 scans. Self-supported samples (20-24 mg/cm²) were put into an infrared cell equipped with a KCl window, designed for treating the samples in a controlled atmosphere. The samples were submitted to the following pretreatment: (i) drying in Ar flow at 120 °C for 1 h; (ii) reduction under flowing hydrogen at a programmed temperature rate (10°C/min) from 120 to 400°C, plus 60 min at 400 °C; (iii) outgassing in Ar at 400°C for 30 min, and finally cooled down in flowing Ar from 400 °C to room temperature. Successive CO pulses in a He flow were sent to the sample, registering the IR spectrum elapsed 5 min after each injection, to follow the formation of the absorption bands. To obtain the IR spectrum corresponding to saturation, a CO flow was used for 5 min, and then outgassing in Ar for 15 min. The spectra presented here were obtained after subtracting the gas phase and solid contributions.

Catalytic activity test

Two different n-butane dehydrogenation tests were carried out, one of them in a continuous flow reactor and the other one in a system where

pulses of *n*-butane were sent to the catalyst. The continuous flow experiment was performed at 500 °C and atmospheric pressure, in a conventional reaction line built in stainless steel. The switching of gases was done without mixing or access of air. A Vycor U-tube (6 mm OD) reactor was charged with 20 mg of catalyst. Samples were pretreated in Ar flow at 120 °C for 1 h and then reduced in H₂ flow at 500 °C for 2 h. The reaction mixture contained *n*-C₄H₁₀ and H₂, with a H₂:*n*-C₄H₁₀ ratio of 10. A total flow of 66 mL/min and a GHSV of 200 L·g⁻¹·h⁻¹ were used. Taking into account that H₂ is a by-product of the dehydrogenation reaction, its presence as a reagent would not be thermodynamically favorable. However, it is very important to include H₂ in the feedstock in order to decrease the carbon formation and hence to moderate the activity decrease along the reaction time [19].

The pulse experiments were performed by injecting pulses of the same hydrogen and *n*-butane mixture, at the same conditions as the continuous flow experiments. The catalytic bed was kept under flowing He (30 mL/min) between the injections of successive pulses. The exit gases were analyzed in a Perkin-Elmer GC, equipped with an Al₂O₃/KCl 50 m x 0.25 mm capillary column and a flame ionization detector (FID).

Specific activity (A), *n*-butane conversion and selectivity were calculated on a carbon basis, using the FID areas (A_{*i*}) and the corresponding response factors (rf_{*i*}), according to the following equations:

$$A (\text{min}^{-1}) = F_{n-C4} \cdot \frac{\text{conversion}}{n_{Pd}}$$

$$\text{Conversion}(\%) = \left[1 - \frac{A_{n-C4} \cdot rf_{n-C4}}{\sum A_i \cdot rf_i} \right] \times 100$$

$$\text{Selectivity} (\%) = \left[\frac{\sum_{i=1}^4 A_{C4s} \cdot rf_{C4s}}{(\sum A_i \cdot rf_i) - A_{n-C4} \cdot rf_{n-C4}} \right] \times 100$$

where F_{n-C4} is the *n*-butane molar flow = 0.000245 mol/min; n_{Pd} = Pd moles in the sample (based on XRF results)

Results and discussion

1. Catalysts characterization

Table 1 shows the values of Pd and Sn loadings obtained by XRF. It is observed that catalysts supported on alumina have a Pd loading near to the nominal composition of 0.5 wt %, meanwhile the ones

supported on silica have lower values of Pd contents (0.31-0.36 wt. %). This could be caused by the low affinity of palladium precursor with silica, hindering the anchoring of Pd anions (as PdCl_n(H₂O)_{4-n-2-n}) on this support [20]. According to Toebe et al. [21], the nature of the interactions of the precursor metal salt with a given support depends on the pH of the solution, the zero point charge (ZPC) of the support, and the nature of ions to be adsorbed. The ZPC varies from 7.0 to 9.0 for γ -alumina, and 1.0 to 2.0 for silica [21]. Therefore, during the impregnation with the Pd solution (PdCl₂ in HCl 0.1 N, pH \approx 1), the surface of the alumina support becomes positively charged, and tends to adsorb compensating anions like PdCl₄²⁻, but the opposite occurs in the case of silica, because of the pH value is in the range of its ZPC. For the case of Sn content, the values were slightly lower than the nominal (0.056 – 0.28 wt. %) for all of the catalysts.

Chlorine contents were also determined by XRF. Only the catalysts supported on alumina showed significant contents of Cl⁻ ions, in the range of 0.54 - 0.70 wt. %, that increased in bimetallic catalysts, i. e., the Cl content increased with the Sn loading, from 0.54 to 0.66%. This fact was expectable, as the Cl⁻ ion sources came from both the Pd and Sn solutions in the preparation of the bimetallic catalysts.

The significant Cl content found in the Al₂O₃-supported catalysts after the calcination treatment at 500 °C for 2 hours, suggests that this anion was initially well anchored to the surface of the alumina, probably as a superficial complex of Pd and chlorine (Pd_xO_yCl_z) which has a high thermal stability [22]. Rodriguez et al. [1] concluded that this palladium superficial complex was also formed during the calcination of Pd-Ga/Al₂O₃ catalysts, considering these species as mobile complexes that spread over the alumina surface, which can improve the Pd dispersion upon reduction.

The BET surface areas (SBET) of some catalysts are also listed in Table 1. Regardless of the amount of Pd and Sn added, the values of BET surface area of the catalysts remain as the corresponding supports (210 m²/g for alumina and 224 m²/g for silica). Similar results were found for pore volumes (values not shown). As expected, the textural properties of the catalysts are almost the same as those of their respective supports, due to small amounts of Pd and Sn on the surface of the alumina and silica.

UV-DRS spectra of Pd-Sn catalysts supported on alumina and silica are presented in Figures 1 and 2, respectively. It can be observed that samples containing palladium (Fig. 1(a) – (d)) display similar spectra, exhibiting bands at 214, 245, 275 and 425 nm.

The band observed at 214 nm can be associated to the charge transfer (Pd \square Cl) of PdCl₂ [22], whereas the strong band at 245 nm is assigned to charge transfer Pd \square O, and the band at 275 nm has been attributed to Pd_xO_yCl_z surface complex [22]. The band at 425 nm is related to d-d transition in PdO species interacting strongly with the alumina support. It is noteworthy that the unsupported PdO phase, exhibits a signal around 490 nm, which was not observed in the spectra shown in Fig. 1. Furthermore, the UV spectrum of the Sn_{0.43}Al sample (Fig. 1e) shows a broad band in the range 225-300 nm. This broad signal is also assigned to the charge transfer Sn \square O [22]. In summary, these results lead to the existence of a Pd and Cl phase on the surface of the support, which can be strongly stabilized.

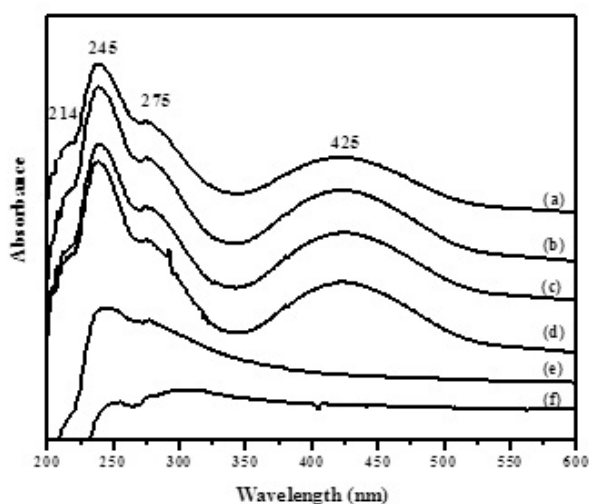


Figure 1. UV-DRS spectra for Al₂O₃-supported catalysts: (a) Pd_{0.40}Al; (b) Pd_{0.55}Sn_{0.045}Al; (c) Pd_{0.52}Sn_{0.091}Al; (d) Pd_{0.54}Sn_{0.19}Al; (e) Sn_{0.43}Al; and (f) Al.

On the other hand, samples supported on silica show UV-DRS spectra different from those observed for the ones supported on alumina. UV-DRS spectrum of Pd_{0.34}Si (Fig. 2a) presented a wide band in the d-d transition region around 490 nm, related to the electronic structure of PdO crystals in supported Pd catalysts [23]. The other signals in the charge transfer region at 250-300 nm are contributions of the silica. In the spectra of the bimetallic Pd_{0.31}Sn_{0.061}Si and Pd_{0.31}Sn_{0.22}Si catalysts (Fig. 2(b) – (c)), similar bands as those in the monometallic Pd_{0.34}Si catalyst can be observed, which indicates the presence of PdO phase without any interaction with the silica support. Finally, the signals at 200-350 nm exhibited for Sn_{0.51}Si sample (Fig. 2d), are ascribed to the Sn \square O charge transfer and silica support.

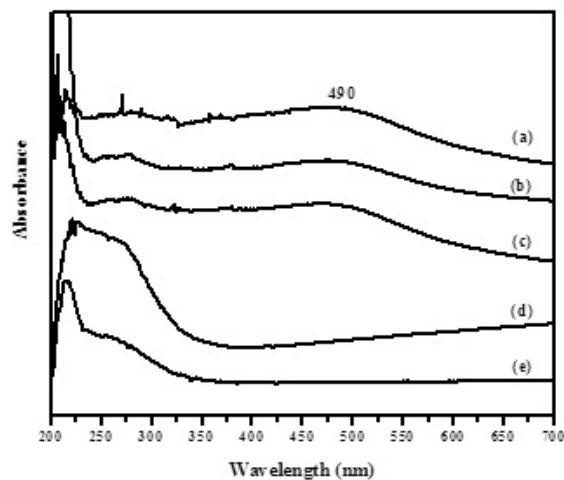


Figure 2. UV-DRS spectra for SiO₂-supported catalysts: (a) Pd_{0.34}Si; (b) Pd_{0.55}Sn_{0.061}Si; (c) Pd_{0.31}Sn_{0.22}Si; (d) Sn_{0.51}Si; and (e) Si.

The TPR profiles of the catalysts supported on alumina are shown in Figure 3. The monometallic and bimetallic Pd-Sn catalysts show very similar reduction profiles (Figs. 3a-3d) with low intensity signals at 19, 50-80, and 300 °C, and a wide and extensive signal in the temperature range of 80-260 °C. The peaks at 19 and 50-80 °C can be assigned to the reduction of crystalline PdO with different sizes, where the largest particles are reduced at lower temperatures [1, 11, 24]. The signal with the great broadness (80-260 °C) has been associated to the reduction of different species of Pd_xO_yCl_z [1, 11], while the peak at 300 °C is attributed to the reduction of PdO particles interacting strongly with the support [25].

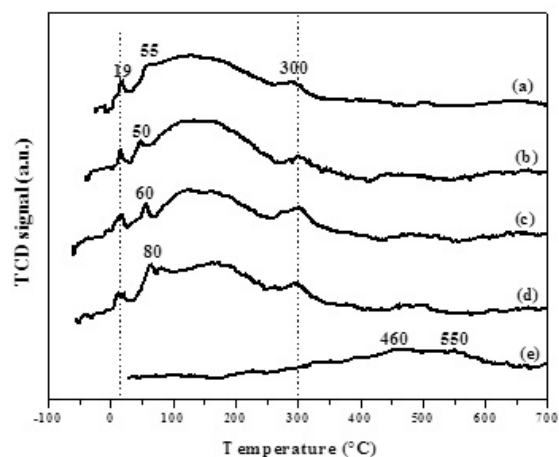


Figure 3. TPR profiles for Al₂O₃-supported catalysts: (a) Pd_{0.40}Al; (b) Pd_{0.55}Sn_{0.045}Al; (c) Pd_{0.52}Sn_{0.091}Al; (d) Pd_{0.54}Sn_{0.19}Al and (e) Sn_{0.43}Al.

For Sn_{0.43}Al sample, a broad reduction signal between 300 and 650 °C is observed. This signal could be attributed to reduction of Sn⁴⁺ to Sn²⁺ and/or SnO [4, 26, 27], so that it indicates some resistance to reduction.

TPR profiles of the catalysts supported on silica are presented in Figure 4. For bimetallic catalysts (Figs. 4b-4d), the reduction peaks observed at low temperatures (< 100 °C), correspond to the reduction of large PdO particles [1, 11, 24], in contrast to that observed in the catalysts supported on alumina. For Pd_{0.34}Si (Fig. 4a), the reduction peaks observed at 21 and 38 °C, could be associated to the reduction of PdO particles with different sizes. In addition, the negative signal at 60 °C is ascribed to the decomposition of β -hydride Pd phase (β -PdHx), whose presence indicates the existence of large palladium particles [24].

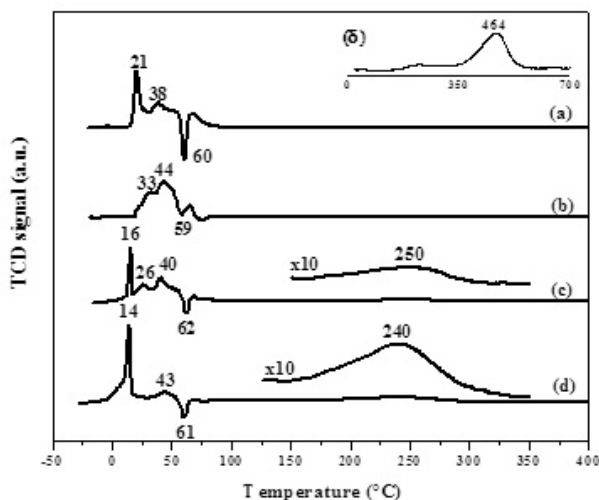


Figure 4. TPR profiles for SiO₂-supported catalysts: (a) Pd_{0.34}Si; (b) Pd_{0.31}Sn_{0.061}Si; (c) Pd_{0.36}Sn_{0.12}Si; (d) Pd_{0.31}Sn_{0.22}Si and (δ) Sn_{0.51}Si (insert)

Some changes occurred in the reducibility of these catalysts when increasing the Sn/Pd ratio. For the Pd_{0.31}Sn_{0.061}Si catalyst, the TPR profile shows signals at 33 and 44 °C, followed by the decomposition of β -hydride Pd phase (PdHx) at 59 °C. For the Pd_{0.36}Sn_{0.12}Si and Pd_{0.31}Sn_{0.22}Si catalysts (Fig. 4(c) – (d)), similar reduction signals to those obtained in the monometallic sample are observed, and can also be attributed to the reduction of PdO particles and decomposition of palladium hydride. However, in these bimetallic samples with the highest Sn/Pd ratio, the negative signal decreases in intensity, probably due to a geometric effect of Sn on palladium ensembles, hindering the β -PdHx phase, either by the formation of bimetallic

Pd-Sn particles [28] or by the dilution of Pd particles by Sn atoms [29].

Other signals centered at 240-250 °C observed for Pd_{0.36}Sn_{0.12}Si and Pd_{0.31}Sn_{0.22}Si catalysts, can be ascribed to the reduction of Sn⁴⁺ catalytically assisted by PdO, thus indicating a close interaction between Pd and Sn in the bimetallic catalysts. As can be seen in the insert in Fig. 4, the reduction of Sn⁴⁺ occurred at higher temperatures (around 464 °C) in the Sn_{0.51}Si sample [27].

The values of CO/Pd ratio obtained from chemisorption measurements are also listed in Table 1. For catalysts supported on alumina, the values of CO/Pd ratio remained in the range of 0.51-0.58, despite of the presence of tin. These results display a high Pd dispersion, probably as a result of the formation of Pd_xO_yCl_z, promoted by the presence of Cl [29]. Pd species were strongly stabilized, which is in agreement with UV-DRS (Fig. 1) and TPR (Fig. 3) results. On the other hand, the high values of the CO/Pd ratio corresponded with that obtained by Daley *et al.* [30], who reported a high Pd dispersion (ca. 50%) when the catalysts were subjected to chlorination treatment, and it was ascribed to the interactions between hydroxyl groups of the support and anions of precursor salt.

For the catalysts supported on silica, the values of CO/Pd ratio were significantly lower. In this case, they were highly dependent on the presence of Sn. For the monometallic Pd_{0.34}Si catalyst, a CO/Pd ratio of 0.20 was obtained, decreasing with the content of tin to 0.06-0.09 for the bimetallic Pd-Sn/SiO₂ catalysts.

The decrease in CO chemisorption with the presence of tin can be attributed to a possible blocking and/or substitution of Pd atoms by Sn and/or the formation of alloys at high tin content [29]. Moreover, the Sn atoms could also cause a weakening of the strength of CO adsorption on Pd. Changes in the stoichiometry of CO adsorption on Pd due to the Sn addition, considering the different forms of adsorbed CO, has been reported by Sales *et al.* [29].

FTIR-CO spectra are presented in Figures 5-8. The results were expressed as a function of CO coverage on Pd (θ_{CO}). For the monometallic catalyst Pd_{0.40}Al (Fig. 5b), four bands were observed at 2155, 2125, 1990 and 1945 cm⁻¹. The intensity of these bands progressively increased with θ_{CO} , and another band arose at 2085 cm⁻¹ when the saturation was reached (Fig. 5f). Besides, the band at 1990 cm⁻¹ shifted to lower frequency (1980 cm⁻¹).

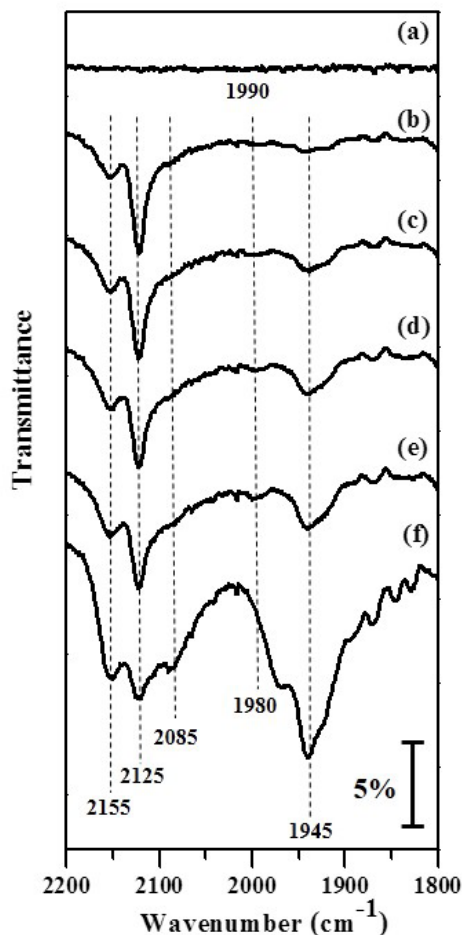


Figure 5. FTIR spectra of CO adsorbed for the Pd_{0.40}Al catalyst at increasing CO coverages: (a) $\theta=0$, (b) $\theta=0.20$, (c) $\theta=0.27$, (d) $\theta=0.31$, (e) $\theta=0.36$ y (f) $\theta=1$.

CO adsorption on supported Pd catalysts depends greatly on the Pd oxidation state [31], and the location of Pd atoms in different Pd crystal planes (111, 100, 110), with different coordination numbers (9, 8, and 7, respectively) [29]. Hence, the band at 2155 cm⁻¹ is attributed to the interaction of CO with residual surface Pd²⁺ ions (linear carbonyls Pd²⁺ - CO), which are stabilized by neighbouring chloride ions, present in all supported alumina catalysts after calcination (Table 1), and were not removed by the reduction treatment (400 °C for 60 min under H₂). The band at 2125 cm⁻¹ was attributed to the linear CO adsorption on Pd⁺ ions [31], which are also stabilized by neighbouring chloride ions. The weak band at 2085 cm⁻¹ is ascribed to linear CO species adsorbed on metallic Pd [32]. The rest of the bands located at 1980 and 1945 cm⁻¹ are ascribed to CO bridged species located on different Pd crystal

planes and/or submitted to dipole-dipole coupling of different intensities. Therefore, the CO:Pd stoichiometry ratio can be far from 1.

In the bimetallic Pd-Sn/Al₂O₃ catalysts, the spectra exhibited the same bands observed for the monometallic one (2155, 2125, 2085, 1990 and 1945 cm⁻¹), but slightly shifted to lower wavenumbers. Thereby, only the infrared spectra obtained for the bimetallic Pd_{0.55}Sn_{0.045}Al catalyst (Sn/Pd = 0.073) are shown (Fig. 6).

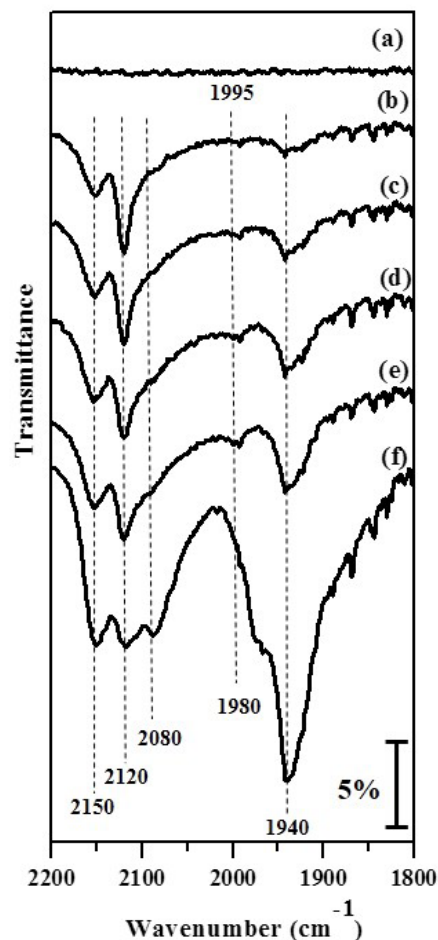


Figure 6. FTIR spectra of CO adsorbed for the Pd_{0.55}Sn_{0.045}Al catalyst at increasing CO coverages: (a) $\theta=0$, (b) $\theta=0.19$, (c) $\theta=0.25$, (d) $\theta=0.30$, (e) $\theta=0.36$ y (f) $\theta=1$.

The assignments of the IR bands for the Al₂O₃-supported catalysts, indicate that a fraction of Pd species remained in oxidized state, as Pd⁺ and/or Pd²⁺, even after reduction at 400 °C in H₂ for 1 h, while the rest of Pd is completely reduced to Pd⁰. It is worth noticing in the FTIR-CO spectra in Figs. 5 and 6 that the intensity of the band in the region

of linear carbonyls is greater than bridged ones, at lower θ_{CO} (Figs. 5b and 6b), i. e., CO is preferentially adsorbed on Pd sites stabilized with Cl⁻ ions. As θ_{CO} increased, Pd⁺ and Pd²⁺ were saturated, allowing to increase CO adsorption on Pd⁰ atoms.

For the silica-supported catalysts, FTIR-CO spectra of monometallic and bimetallic catalyst are shown in Figures 7 and 8, respectively. For the Pd_{0.34}Si catalyst, bands are observed initially at 2087 and 1905 cm⁻¹ (Fig. 7b). As θ_{CO} increased, a band appeared at 1990 cm⁻¹, and then the bands at 1905 and 1990 cm⁻¹ become shoulders, which are overlapped with a new band at 1975 cm⁻¹ when saturation was reached. The band at 2087 cm⁻¹ is assigned to the linear adsorption of CO on metallic Pd [32], while the bands located between 1990 and 1905 cm⁻¹ are ascribed to bridged CO species, also over metallic Pd [29, 32]. According to the spectrum in Fig. 7f, there is a higher proportion of bridged CO (COB) than linear CO (COL) species, resulting in a value of COL/COB ratio of 0.30 after integration of the signals, which indicates the largest Pd ensembles in this sample.

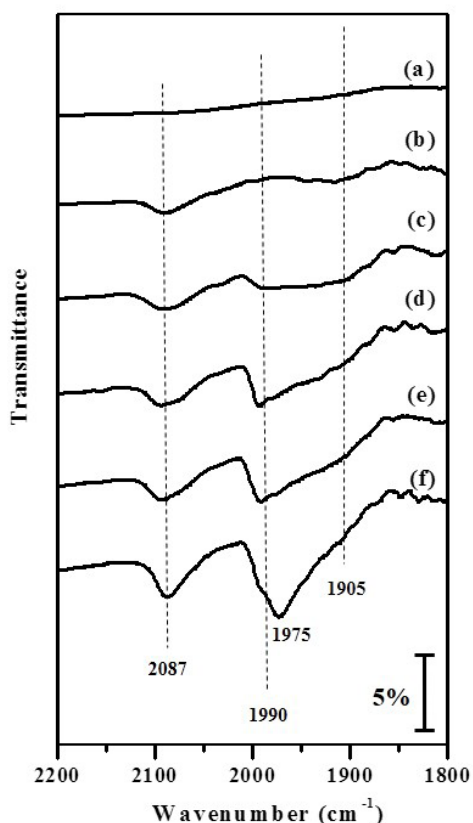


Figure 7. FTIR spectra of CO adsorbed for the Pd_{0.34}Si catalyst at increasing CO coverages: (a) $\theta=0$, (b) $\theta=0.23$, (c) $\theta=0.43$, (d) $\theta=0.67$, (e) $\theta=0.72$ y (f) $\theta=1$.

However, for the bimetallic catalysts (Fig. 8), the COL/COB ratio increased from 0.30 to 0.68. This is explained by a dilution of Pd by Sn on the catalyst surface layer, and an ensemble effect should account for the preferential suppression of bridged CO species which requires the presence of adjacent Pd atoms [29, 32]. Nevertheless, the presence of tin seems to weaken the CO adsorption strength, as linear entities are less firmly bonded than bridged ones.

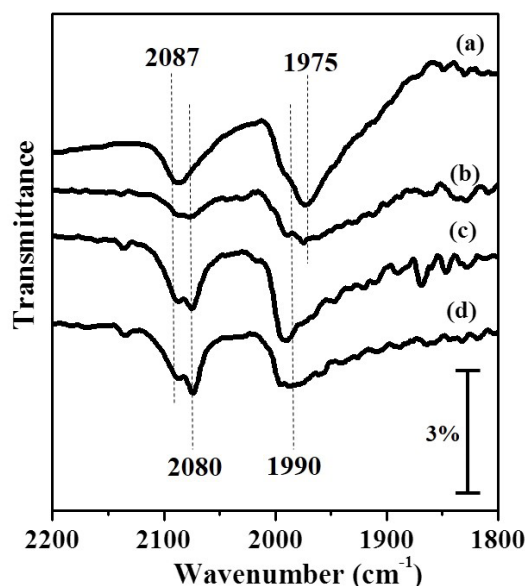


Figure 8. FTIR spectra of CO adsorbed for the samples after saturation ($\theta_{CO}=1$) with flowing CO: (a) Pd_{0.34}Si; (b) Pd_{0.31}Sn_{0.061}Si; (c) Pd_{0.36}Sn_{0.12}Si and (d) Pd_{0.31}Sn_{0.22}Si.

On the other hand, the maxima of the signals in FTIR-CO spectra tend to change progressively with the Sn/Pd atomic ratio, i.e., peaks initially located at 2087 and 1975 cm⁻¹ for the monometallic Pd_{0.34}Si, shifted to 2080 and 1990 cm⁻¹, respectively, for the bimetallic Pd-Sn/SiO₂ catalysts. Therefore, the presence of tin can be affecting the electronic properties of palladium in these silica-supported catalysts [32].

2. Catalytic activity measurements.

2.1 Continuous flow reactor

The measurements were carried out at 500 °C in a differential flow reactor (n-butane conversion less than 10%), and the results were expressed as moles of n-butane converted per mole of Pd per minute, i.e., specific activity (min⁻¹), as a function of time on-stream (TOS). It is known that dehydrogenation

reactions are metal-catalyzed non-demanding reactions [33]. On the other hand, it is important to indicate that the $\text{Sn}_{0.43}\text{Al}$ and $\text{Sn}_{0.51}\text{Si}$ catalysts did not exhibit catalytic activity for the n-butane dehydrogenation under the reaction conditions.

The specific activity of the Al_2O_3 -supported catalysts as a function of TOS is shown in Fig. 9. The $\text{Pd}_{0.40}\text{Al}$ catalyst displayed an initial specific activity of 44 min^{-1} , suffering a fast deactivation in the first 15 min of TOS, and then the activity decreased progressively along the reaction time. Deactivation was also observed in the rest of the catalysts, probably as a result of coke deposition on the catalyst surface [19]. At these reaction conditions, the formation of coke would build up on both the metal and support sites [34, 35]. However, at the beginning of the reaction, first coke is deposited on Pd atoms of high coordination number (cluster or ensembles) and, then, coke blocks the Pd atoms of low coordination number like corners or edges. Therefore, low coordinated Pd palladium atoms are more resistant to deactivation by coke [35].

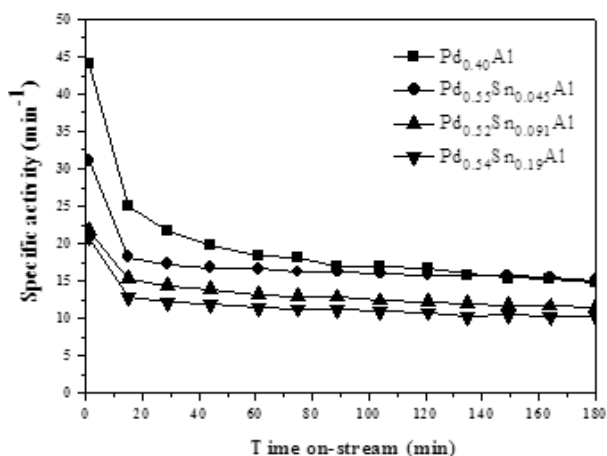


Figure 9. Specific activity at $500 \text{ }^\circ\text{C}$ as a function of TOS for the Al_2O_3 -supported catalysts.

The initial activity and deactivation rate decreased upon Sn addition, in good agreement with that observed by other researchers in Pt-Sn [4] and Pd-Sn catalysts [10]. This deactivation occurred mainly in the first 15 minutes of TOS, and the catalyst with the highest Sn content ($\text{Pd}_{0.54}\text{Sn}_{0.19}\text{Al}$, Sn/Pd = 0.32) displayed the smallest activity. These effects of the Sn addition on the catalytic behavior of Pd supported on alumina can be explained mainly in terms of geometric effects, as the majority of Sn in the bimetallic catalysts blocked the Pd atoms of high coordination number. Besides, the FTIR-CO results (Figs. 5 and 6) show the lack of any electronic effect

of tin on palladium, probably because the electronic properties of palladium were already modified by the presence of chlorine.

Fig. 10 shows the specific activity for n-butane dehydrogenation on SiO_2 -supported catalysts. Specific activities of these catalysts were lower than those obtained in alumina supported catalysts (Fig. 9). The $\text{Pd}_{0.34}\text{Si}$ catalyst exhibited an initial activity of 31 min^{-1} , then the activity decreased monotonically with TOS. The addition of a small amount of Sn ($\text{Pd}_{0.31}\text{Sn}_{0.061}\text{Si}$) decreased the initial activity, but after 15 min of TOS, this catalyst showed the same activity as the monometallic one.

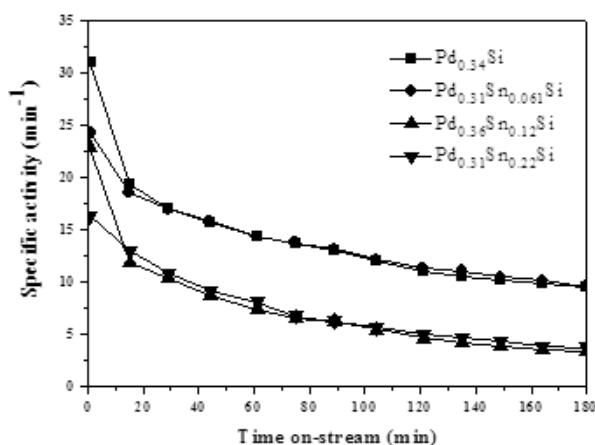


Figure 10. Specific activity at $500 \text{ }^\circ\text{C}$ as a function of TOS for the SiO_2 -supported catalysts.

The addition of a greater amount of Sn (Sn/Pd = 0.30 and 0.64) decreased the catalytic activity from initial values of 23 and 16 min^{-1} , respectively, to final values around 3 min^{-1} . This decrease can be attributed to both geometric and electronic effects of Sn on Pd in concordance with CO chemisorption and FTIR-CO results. Moreover, TPR results suggested that Pd and Sn were in intimate contact on this support, due to the possible formation of bimetallic Pd-Sn particles after reduction. In the silica-supported Pd catalysts, predominates the existence of high coordination Pd atoms, indicated by the low Pd dispersion (CO measurements). Furthermore, all of the silica-supported Pd catalysts were deactivated at the same extent in spite of the presence of Sn (Fig. 10).

Table 2 compiles the selectivity to all butenes (initial: SD,₀ and final: SD,_f), selectivity to isomerization (initial: SI,₀ and final: SI,_f) and the deactivation parameter $\Delta R/\text{RO}$, where ΔR is the difference between the final and initial reaction rates (RO and R_f, respectively).

Table 2. Initial and final selectivity for dehydrogenation (SD,o, SD,f), selectivity for isomerization (SI,o, SI,f) and deactivation parameter ($\Delta R/RO$; ΔR : initial reaction rate [RO]–final reaction rate [Rf]) in the continuous flow reactor at 500 °C.

Catalyst	S _{D,o}	S _{D,f}	S _{I,o}	S _{I,f}	$\Delta R/R^o$ (%)
Pd _{0.40} Al	50	89	3	4	40
Pd _{0.55} Sn _{0.045} Al	44	83	3	4	17
Pd _{0.52} Sn _{0.091} Al	63	92	3	3	25
Pd _{0.54} Sn _{0.19} Al	68	94	2	2	20
Pd _{0.34} Si	77	98	-	-	51
Pd _{0.31} Sn _{0.061} Si	100	100	-	-	48
Pd _{0.36} Sn _{0.12} Si	100	100	-	-	72
Pd _{0.31} Sn _{0.22} Si	100	100	-	-	71

SD,o, SI,o: measured at 1 min of the reaction beginning. SD,f, SI,f: measured at 180 min of time of stream.

Ro: measured at 15 min of the reaction beginning. Rf: measured at 180 min of time of stream.

The addition of Sn decreased the $\Delta R/RO$ values only in the Al₂O₃-supported Pd catalysts, and this decrease seems to be determined by the minimum quantity of the promoter added. For the Al₂O₃-supported catalysts, the deactivation parameter values are similar to that obtained by Ballarini *et al.* [19] and Bocanegra *et al.* [36] in monometallic Pt(0.5%) and bimetallic Pt(0.5%)Sn(0.3%) catalysts supported on γ -Al₂O₃/ α -Al₂O₃ and MgAl₂O₄, respectively. In the case of SiO₂-supported catalysts, the surface modification caused by Sn affected structure-sensitive reactions, such as hydrogenolysis rather than coking.

The Sn addition increased the selectivity toward butenes in both Al₂O₃- and SiO₂-supported catalysts. For the Pd-Sn/Al₂O₃ catalysts, the selectivity increased with the Sn content and the time on-stream, achieving a selectivity of 94% for the Pd_{0.54}Sn_{0.19}Al catalysts at 180 min of TOS; probably Sn and coke blocked the most active Pd sites, responsible for the reactions leading to hydrogenolysis. Pd in the PdxClyOx phase appears to be the most active species, because the electronic properties of Pd were modified by means of charge transfer Pd□Cl [22]. It should be pointed out that an electronic effect of Sn on Pd was not observed for this series of catalyst. In addition to dehydrogenation and hydrogenolysis products, isobutene was also observed: an isomerization selectivity between 2-4 % was registered in all Pd-Sn/Al₂O₃ catalysts [37].

For the silica-supported catalysts, higher selectivity values toward butenes were observed. The monometallic Pd_{0.34}Si exhibited dehydrogenation selectivity of 77 % at the beginning (1 min) and 98% at the end (180 min of TOS) of the experiment. These results indicate that Pd in metallic state (Pd⁰), as in the silica support, exhibits high selectivity toward dehydrogenation. In all Pd-Sn/SiO₂ catalysts, the

dehydrogenation selectivity was 100 %. The SiO₂-supported catalyst with the lowest Sn loading (Sn/Pd = 0.18) showed the best performance of these catalysts, considering both the selectivity toward butenes and the dehydrogenation activity. It is worth mentioning that isobutene was not observed as a product, probably due to the low acidity of the support, that could not catalyze skeletal isomerization reactions.

2.2 Pulse experiments.

In order to elucidate the catalytic behavior for n-butane dehydrogenation over the different mono and bimetallic supported catalysts during the first steps of reaction, a study of the catalytic performance was carried out by sending pulses of the H₂/n-butane reactant mixture to the reactor.

The n-butane conversion for the indicated Al₂O₃- and SiO₂-supported Pd-Sn catalysts as a function of the number of H₂/n-butane pulses, are shown in Figure 11. For the Al₂O₃-supported catalysts, it can be seen that the Pd_{0.40}Al sample showed a conversion of 49% in the 1st pulse and 43% in the 12th pulse, while the Pd_{0.55}Sn_{0.045}Al and Pd_{0.54}Sn_{0.19}Al catalysts showed higher conversions of 64-68% in the 1st pulse and 46-47% in the 12th pulse. The lower conversion obtained on the Pd_{0.40}Al catalyst is due to the smaller amount of Pd atoms exposed on the surface, considering both the lower Pd loading and the similar Pd dispersion (Table 1). The conversion for the bimetallic catalysts supported on alumina are in agreement to CO chemisorption results (Table 1), where the CO/Pd ratio was unaffected by the Sn content. Therefore, conversion values observed in Figure 11 confirm that Pd active sites were unaffected by Sn. Also, the conversion decreases with pulse number, due to the

significant coke deposition at this stage. This fact was also observed by Pirngruber et al. [37] in their studies of n-butane dehydroisomerization.

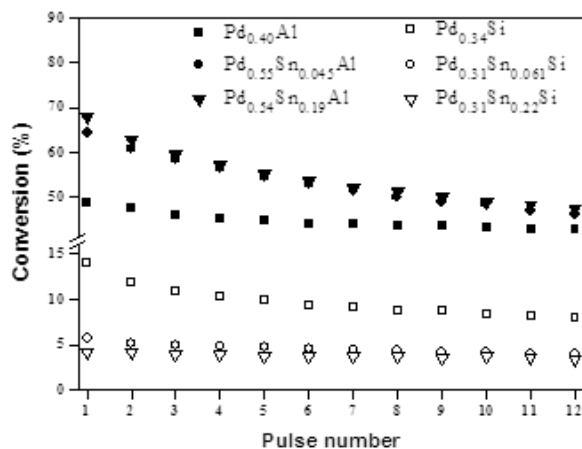


Figure 11. n-butane conversion at 500 °C as a function of the pulse number for the indicated catalysts.

In the case of the catalysts supported on silica, the Pd_{0.34}Si sample showed a conversion of 14% in the 1st pulse, and then gradually decreases with subsequent pulses, until reaching about 8% in the 12th pulse. For the Pd_{0.31}Sn_{0.061}Si and Pd_{0.31}Sn_{0.22}Si catalysts, lower conversion values

were obtained, ranging between 3-6% along the twelve pulses sent to the reactor. In this case, the n-butane conversion decreased with the Sn loading (or Sn/Pd atomic ratio). Similar to the continuous flow experiments, the catalytic activity of the SiO₂-supported catalysts were lower than the Al₂O₃-supported ones, but it should be taken in account that both Pd loading and dispersion were lower in these catalysts (Pd = 0.31-0.34% and CO/Pd = 0.06-0.20, respectively). The decrease in n-butane conversion with the amount of Sn is in agreement with CO/Pd ratio. Nevertheless, the lower deactivation degree in the n-butane dehydrogenation with the pulse number indicates a lower coke deposition rate in these catalysts.

The initial and final selectivity for the n-butane dehydrogenation in pulse experiments are listed in Table 3. For the Al₂O₃-supported catalysts, was observed a high selectivity for hydrogenolysis in all of the pulses of reactant mixture sent to the reactor, while the selectivity toward butenes were unaffected by Sn content, ranging from 2-4% in the 1st pulse and 5-8% in the 12th pulse, which means that, as mentioned above, in the course of the reaction coke deposition affected the hydrogenolysis reactions. On the other hand, it is worth noticing that the deactivation parameter increased in the bimetallic catalysts, from 12 to 28-31%, but this change was attributed to a higher amount of Pd active sites available for the reaction (and, thus, the higher coke formation rate) rather than the presence of Sn.

Table 3. Initial^a and final^b selectivity for dehydrogenation (S_{D,o}, S_{D,f}), selectivity for hydrogenolysis (S_{H,o}, S_{H,f}) and deactivation parameter ($\Delta X/X^o$; ΔX : initial conversion [X_o]–final conversion [X_f]) in the pulse experiments at 500 °C.

Catalyst	S _{D,o}	S _{D,f}	S _{H,o}	S _{H,f}	$\Delta X/X^o$ (%)
Pd _{0.40} Al	4	8	96	92	12
Pd _{0.55} Sn _{0.045} Al	2	5	98	95	28
Pd _{0.54} Sn _{0.19} Al	2	6	98	94	31
Pd _{0.34} Si	19	29	81	71	43
Pd _{0.31} Sn _{0.061} Si	72	90	28	10	31
Pd _{0.31} Sn _{0.22} Si	78	89	22	11	19

a: measured at 1st pulse of the reactant mixture.

b: measured at 12th pulse of the reactant mixture.

For the catalysts supported on silica, all of them exhibited higher selectivity toward butenes, especially the bimetallic ones. The monometallic catalyst showed a selectivity to dehydrogenation between 19-29 %, meanwhile selectivity values were from 72% to 90% for the bimetallic catalysts. As it was expected from previous results (Table 1, Fig. 10), deactivation parameter decreased with Sn content

in these catalysts, from 43 to 19 %, as an evidence of Pd-Sn interactions on the surface of the silica.

The differences in the selectivity between the catalysts supported on alumina and those supported on silica, point out the support's role in Pd active sites. From results obtained in the pulse experiments, it can be concluded that coke deposition rate was lower in the catalysts supported on silica, and the

selectivity toward butenes increased with the Sn addition. These results are explained by a geometric and electronic effects of Sn on Pd, through the dilution of Pd ensembles and the change in the Pd nature upon Sn addition.

From results discussed above, it could be proposed a model of the arrangement of metal particles on the surface of the alumina and silica, in bimetallic catalysts. On alumina, Pd atoms are highly stabilized by chlorine species, which increased d-state vacancies due to a charge transfer from palladium to chlorine, as it was mentioned in the UV-DRS results of these solids (Figure 1), which in turn hinder the Pd-Sn interactions. The representation of these particles on the surface of alumina is schematized in Fig. 12, where two groups of Pd sites predominate: "sites A" representing the Pd particles interacting with Cl- by means of $Pd_xO_yCl_z$ surface complex, and "sites B" representing the Pd particles interacting with Sn. Most of the Pd is included in "site A", which explains why similar characterization results were obtained (UV-DRS, TPR, CO chemisorption, FTIR-CO). Also, these Pd species are the most active in the n-butane dehydrogenation, and the strength of n-butane adsorption on Pd is high enough to favor the rupture of C-C (cracking) rather than C-H (dehydrogenation) bonds [9]. Instead, on "sites B" Pd particles are free of Cl, allowing the interaction with Sn, and represent the minority of Pd. On this type of sites, the hydrocarbon adsorption is weakened, hindering C-C bond ruptures, and favoring the dehydrogenation reactions toward butenes. During the n-butane dehydrogenation in continuous flow reactor, "sites A" were blocked by coke deposition at the beginning (first 15 min of TOS) and, then, the reaction proceeded on "sites B", where differences in catalytic performance of the Al_2O_3 -supported catalysts upon Sn addition were observed. This statement is supported by FTIR-CO results, which indicated that CO is preferentially absorbed on Pd^+/Pd^{2+} species.

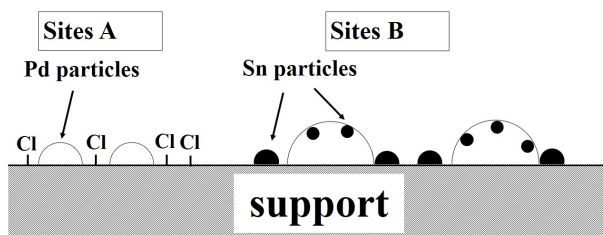


Figure 12. Schematic representation of the distribution of metal particles on the surface of the supports.

On silica, only the "sites B" predominates, as the characterization results (XRF, UV-DRS, TPR and FTIR-CO) showed the absence of any chlorinated

species, and the existence of large Pd ensembles, which showed lower activity and higher selectivity toward butenes and coking. Therefore, it is proposed that both geometry and electronic effects of Sn on Pd are involved in the catalysts supported on silica.

The results obtained herein showed a commitment in the activity-selectivity relationship for the n-butane dehydrogenation. In a continuous flow reactor, Al_2O_3 -supported catalysts displayed better activity and stability for TOS higher than 15 min, with a selectivity toward butenes up to 94% for the $Pd_{0.54}Sn_{0.19}Al$ catalyst. In the case of the SiO_2 -supported catalysts, all the samples displayed a high dehydrogenation selectivity (100%), but low activity and the worse stability on TOS.

Conclusions

The Pd species present in the Pd and Pd-Sn supported catalysts depends on the nature of the support. In this sense, when supported on alumina, palladium exists primarily in two forms: (i) as Pd oxychloride ($Pd_xCl_yO_z$), where the electronic properties of the metal are modified by the presence of chlorine, by means of a charge transfer $Pd \square Cl$. This phase is highly resistant to reduction, as some of the palladium species remained as Pd^+/Pd^{2+} even after reduction at 400°C for 1 h. Besides, this Pd-Cl interaction leads to a high metal dispersion and high activity in the n-butane dehydrogenation, but poor selectivity towards butenes; (ii) as Pd metallic (Pd), where a Pd-Sn interaction can be involved, and a higher selectivity toward butenes can be obtained. Over silica, only PdO exists after reduction, with a very low dispersion and activity. The Al_2O_3 -supported bimetallic (Pd-Sn) catalysts showed a better behavior for n-butane dehydrogenation than the SiO_2 -supported ones, considering both the activity and stability. Also, high selective toward butenes was observed for the $Pd_{0.54}Sn_{0.19}Al$ catalysts ($Sn/Pd = 0.32$). These catalysts showed the best performance for n-butane dehydrogenation between all catalysts investigated here.

In spite of the poor performance showed by the SiO_2 -supported catalysts, a better Pd-Sn interaction was evidence in these catalysts. The performance of the Al_2O_3 -supported catalysts tested herein for n-butane dehydrogenation can be compared with the Pt-base catalysts, which encourages to further studies of the supported Pd catalysts for this reaction.

Acknowledgements

This research was partially supported by the Consejo de Desarrollo Científico y Humanístico of the Universidad del Zulia (CONDES), Venezuela,

under the Projects CC-0145-08 and CC-0090-12. The authors also thanks to Dr. Alberto Campos, of the Laboratorio de Desarrollo de Métodos de Análisis, of the Facultad Experimental de Ciencias de la Universidad del Zulia, by his assistance in the chemical analysis of the catalysts.

References

- RODRIGUEZ, L., ROMERO, D., RODRIGUEZ, D. SANCHEZ, J., DOMINGUEZ, F. ARTEAGA, G. *Appl. Catal. A: Gen* 373:66-70.2010.
- MIRACCA, I., PIOVESAN, L. *Catal. Today* 52: 259. 1999.
- KOBAYASHI, S., KANEKO, S., OHSHIMA, M., KUROKAWA, H., MIURA, H. *Appl.Catal. A: Gen* 417- 418:306- 312. 2012.
- RODRÍGUEZ, D., SÁNCHEZ, J., ARTEAGA, G. *J. Mol. Catal.* 228:309-317. 2005.
- SAHEBDELFAH, S., TAKHTRAVANCHI, M., TAHRIRIZANGENEH, F., MEHRAZMA, S., RAJABI, S. *Chem. Eng. Res. Des.* 90:1090-1097. 2012
- IGLESIAS-JUEZ, A., BEALE, A., MAALJEN, K., CHIENWENG, T., GLATZEL, P., WECKHUYSEN, B. *J. Catal.* 276:268-279. 2010.
- KANEKO, S., ARAKAWA, T., OHSHIMA, M., KUROKAWA, H., MIURA, H. *Appl. Catal. A: Gen* 356:80-87. 2009.
- PISDUANGDAW, S., PANPRANOT, J., METHASTIDSOOK, M., CHAISUK, C., FAUNGNAWAKIJ, K., PRASERTHDAM, P., MEKASUWANDUMRONG, O. *Appl. Catal. A: Gen* 370:1. 2009**
- Mendez, J., Rodriguez, D., Sanchez, J. Arteaga, G. *Ciencia* 20:132-141. 2012.
- VALECILLOS, J., RODRÍGUEZ, D., MENDEZ, J., SOLANO, R., GONZÁLEZ, C. ACOSTA, T., SÁNCHEZ, J., ARTEAGA, G. *Ciencia* 14 (Special Number):1.2006.
- VIRLA, L., MEDINA, V., RODRÍGUEZ, D., SOLANO, R., MENDEZ, J., ARTEAGA, G. *FARAUTE Ciens. y Tec.* 4(2):68-77. 2009.
- HAMID, S., ARUN KUMAR, M., LEE, W. *Appl. Catal. B: Environ* 187:37-46. 2016.
- PIZARRO, A.H., MOLINA, C.B., RODRIGUEZ, J.J., EPRON, F. *J. Environ. Chem. Eng.* 3: 2777-2785. 2015.
- LIN, W., LIN, L., ZHU, Y.X., XIE, Y.C., SCHEURELL, K., KEMNITZ, E. *Appl. Catal. B* 57:175-181. 2004.
- LOVÓN-QUINTANA, J.J., SANTOS, J.B.O., LOVÓN, A.S.P., LA-SALVIA, N., VALENÇA, G.P. *J. Mol. Catal. A: Chem.* 411:117-127. 2016
- ZHAO, J., XU, X., LI, X., WANG, J. *Catal. Commun.* 43:102-106. 2014.
- VICENTE, A., LAFAYE, G., ESPECEL, C., MARÉCOT, P., WILLIAMS, C.T. *J. Catal.* 283:133-142. 2011.
- PATTAMAKOMSAN, K., EHRET, E., MORFIN, F., GÉLIN, P., JUGNET, Y., PRAKASH, S., BERTOLINI, J. C., PANPRANOT, J., CADETE, SANTOS AIRES, F. *J. Catal. Today* 164:28-33. 2011.
- BALLARINI, A.D., ZGOLICZ, P., VILELLA, I.M.J., DE MIGUEL, S.R., CASTRO, A.A., SCELZA, O.A. *Appl. Catal. A: Gen* 381:83-91. 2010.
- ELDING, L.I., OLSSON, L.F. *J. Phys. Chem.* 82:69-74. 1978
- TOEBES, M. L., VAN DILLEN, J. A., DE JONG, K. P. *J. Mol. Catal. A: Chem* 173:75-98. 2001.
- GASPAR, A. B., DIEGUEZ, L. C. *Appl. Catal. A: Gen* 201:241-251. 2000.
- FERRER, V., FINOL, D., RODRIGUEZ, D., DOMINGUEZ, F., SOLANO, R., ZÁRRAGA, J., SÁNCHEZ, J. *Catal. Lett.* 132:292-298. 2009.
- FERRER, V., MORONTA, A., SÁNCHEZ, J., SOLANO, R., BERNAL, S., FINOL, D. *Catal. Today* 107-108:487-492. 2005
- FERRER, V., FINOL, D., SOLANO, R., MORONTA, A., RAMOS. M. *J. Environ Sci.* 27:87-96. 2015.
- LIESKE, H., VÖLTER. J. *J. Catal.* 90:96-105. 1984.
- DAUTZENBERG, F. M., HELLE, J. N., BILOEN, P., SACHTLER. W. M. H. *J. Catal.* 63:119-128. 1984
- LEE, A.F., BADDELEY, C.J., TIKHOV, M.S., LAMBERT, R.M. *Surf. Sci.* 373:195-209. 1997.
- SALES, E.A., JOVE, J., MENDES, M.J., BOZON-VERDURAZ, F. *J. Catal.* 195:88-95. 2000.
- DALEY, R.A., CHRISTOU, S.Y., EFSTATHIOU, A.M., ANDERSON, J.A. *Appl. Catal. B: Environ* 60:117-127. 2005.

-
31. VALDEN, M., KEISKI, R. L., XIANG, N., PERE, J., AALTONEN, J., PESSA, M., MAUNULA, T., SAVIMÄKI, A., LAHTI, A., HÄRKÖNEN, M. **J. Catal.** 161:614-625. 1996.
 32. SCIRÈ, S., BURGIO, G., CRISAFULLI, C., MINICÒ, S. **Appl. Catal. A: Gen** 274:151-157. 2004.
 33. MAZZIERI, V. A., GRAU, J. M., YORI, J. C., VERA, C. R., PIECK, C. L. **App. Catal. A: Gen** 354:161-168. 2009.
 34. SRIHIRANPULLOP, S., PRASERTHDAM, P. **Catal. Today** 93-95:723-727. 2004.
 35. MARECOT, P., AKHACHANE, A., MICHEAUD, C., BARBIER, J. **Appl. Catal. A: Gen** 169:189-196. 1998.
 36. BOCANEGRA, S.A., GUERRERO-RUIZ, A., DE MIGUEL, S.R., SCELZA, O.A. **Appl. Catal. A: Gen** 277:11-22. 2004.
 37. PIRNGRUBER, G. D., SESHAN, K., LERCHER, J. A. **J. Catal.** 186:188-200. 1999



UNIVERSIDAD
DEL ZULIA

CIENCIA

Vol.26 N°1, 2

*Esta revista fue editada en formato digital y publicada
en junio de 2018, por el Fondo Editorial Serbiluz,
Universidad del Zulia. Maracaibo-Venezuela*

www.luz.edu.ve
www.serbi.luz.edu.ve
produccioncientifica.luz.edu.ve